Zhou et al. Nanoscale Research Letters
DOI 10.1186/s11671-015-0754-1

Nanoscale Research Letters
a SpringerOpen Journal

NANO EXPRESS Open Access

Enhanced efficiency of inverted polymer solar cells by using solution-processed TiO_x/CsO_x cathode buffer layer

Xiaodong Zhou[1*], Xi Fan[2], Xianke Sun[1], Yunli Zhang[1] and Ziqiang Zhu[1]

Abstract

In this work, a double-buffer film of TiO_x coated with CsO_x (TiO_x/CsO_x) was solution prepared to be applied in poly (3-hexylthiophene):indene-C_{60} bisadduct (P3HT:ICBA) and P3HT:[6,6]-phenyl-C_{61}-butyric acid methyl ester (PCBM) inverted polymer solar cells (PSCs). Compared with TiO_x films and CsO_x films, the TiO_x/CsO_x double-buffer film exhibited a favorable energy-level alignment among TiO_x, CsO_x, and the electron acceptor of PCBM or ICBA a better surface morphology; and an enhanced wetting and adhesion property with a contact angle of 21.0°, leading to a higher electron mobility of 5.52×10^{-3} cm^2 $V^{-1} \cdot s^{-1}$. Moreover, the P3HT:ICBA and P3HT:PCBM photovoltaic devices with the double-buffer film showed the best power conversion efficiency up to 5.65% and 3.76%, respectively. Our results not only present that the double-buffer film is superior than the single film of TiO_x and CsO_x, but also imply that the solution-processed film has a potential to be generally used in roll-to-roll processed organic photovoltaic devices.

Keywords: Inverted polymer solar cell; Solution processed; Cathode buffer layer

Background

Polymer solar cells (PSCs) have been a hot research topic due to their advantages of low cost, light weight, and large area [1-4]. Recently, normal (not inverted) PSCs with a considerable power conversion efficiency (PCE) of 7% ~ 9% have been reported [5-15]. In such normal PSCs, however, aqueous poly(3,4-ethylenedioxythiophene):poly(styrenesulfonate) (PEDOT:PSS) dispersion is acidic at pH 1 and corrosive to indium tin oxide substrates [16]; In addition, PSS and Al could diffuse into active layers and react with organic active layers [17]; therefore, instability of PSC devices caused by the anode buffer layer of PEDOT:PSS and the Al cathode has become a main concern for practical applications. To overcome the problems, stable inverted PSCs are widely developed by using metal oxides as buffer layers, e.g., zinc oxide (ZnO) [18-20] and titanium oxide (TiO_x) [21-23] were widely selected as a cathode buffer layer (CBL), whereas MoO_3 was usually employed as an anode buffer layer to replace PEDOT:PSS and to prevent the diffusing of Al atoms into active layers in inverted PSCs [24].

In inverted PSCs, CBLs play a key role of determining device performance. Generally, for efficient PSCs, a good CBL often satisfies several criteria: high transparency, low work function (WF), and favorable energy levels matched well with those of electron acceptors. 1) High-transparency benefits to large light absorption of active layers, thereby leading to more exciton dissociation at the interface of donor/acceptor and an increase in short current density (J_{SC}). 2) As reported in previous literatures [25-27], open circle voltage (V_{OC}) is determined mostly by the energy-level difference between the highest occupied molecular orbital (HOMO) of the donor and the lowest unoccupied molecular orbital (LUMO) of the acceptor [11,12] and the work function difference of the cathode/anode [25-27], as well as the weight ratio of the donor and acceptor [28]. Low work functions of film could increase the work function difference of the cathode/anode and thus leading to an increase in V_{OC} of PSCs [25-27]. Afterwards, the films of low WFs facilitate electron collection by cathodes and restrain the charge

* Correspondence: xdzhou516@163.com
[1]School of Physics and Electromechnical Engineering, Zhoukou Normal University, Zhoukou 466001, People's Republic of China
Full list of author information is available at the end of the article

carrier recombination at the interface of the active layer and film [25,27]. 3) Energy levels of the films, matched well with LUMO and HOMO energies of the components of active layers, could effectively select electrons and block holes, leading to an increase in J_{SC} of PSCs [18-23]. However, is there another factor of the films that has a significant effect on the device performance? Will the contact property of interfaces between active layer droplets and cathode buffer layers be changed when the buffer layer is modified? How will the changes of the interfacial contact property affect the charge carrier mobility and the device performance?

Recently, many films, such as TiO_x [21-23], ZnO [18-20], cesium oxide (CsO_x) [29], Ca [30,31], LiF [32], and self-assembled monolayers [18,33], are widely employed to modify the cathode surfaces in inverted PSCs. Among these films, much attention in the development of inverted PSCs has been focused on TiO_x, which has the advantages of excellent chemical and thermal stability, environmentally friendly, high-electron mobility, and easy fabrication [34]. The TiO_x film is often prepared by sol-gel synthesis [22], atomic layer deposition [23], and thermal-annealed titanium chelate [16]. Moreover, the film can serve as an effective hole- and exciton-blocking layer because of its conduction band of approximately 4.4 eV, which is much higher than the HOMO values of electron acceptor materials [35,36] (seen in Figure 1b). However, challenges still remain for the film, mainly due to the film work function of 4.14 to 4.22 eV [37] still not being low enough for a high V_{OC} in inverted PSCs. The work function commonly affects the work function of cathode and the work function difference of cathode/anode. Thus, the V_{OC} of poly(3-hexylthiophene):[6,6]-phenyl-C_{61}-butyric acid methyl ester (P3HT:PCBM) inverted PSCs with a TiO_x film was usually limited to a small range of 0.55 to 0.58 V under simulated 100-mW cm^{-2} (AM 1.5 G) solar irradiation [23,38], which blocks its practical application in high-efficiency inverted PSCs.

Besides, a CsO_x thin film is commonly prepared by evaporating deposition of Cs_2CO_3 particles or spin coating the Cs_2CO_3 solution. Attributed to the CsO_x is a much lower WF of approximately 2.20 eV as reported in previous literature [27]; it not only can modify the work function of the cathode and cathode buffer layer, but also facilitates electron transportation from electron acceptor materials to the CsO_x surfaces. Therefore, it is believed that CsO_x could be an effective cathode buffer layer for PSCs.

In the work, a solution-processed CsO_x film was inserted at the interface of the active layer/TiO_x. The MoO_3 film with a thickness of 8 to 10 nm was found to be an optimized value [39]. Here, the Al modified by a 10-nm-thick MoO_3 film was evaporated. By increasing

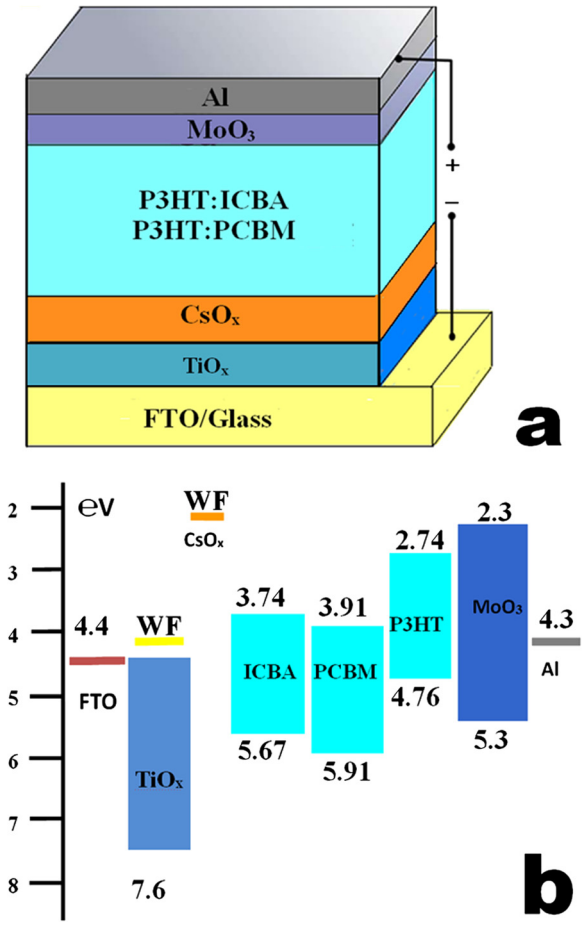

Figure 1 Device structure and schematic energy diagram. **(a)** Device structure of the P3HT:ICBA inverted PSCs and the P3HT:PCBM inverted PSCs. **(b)** Schematic energy diagram of the materials involved in the inverted PSCs.

the work function difference of the cathode/anode, a larger V_{OC} and an enhanced PCE were achieved in P3HT:indene-C_{60} bisadduct (ICBA)-based inverted PSCs and in P3HT:PCBM-based inverted PSCs. First, atomic force microscopy (AFM) measurements present that the double film exhibits a smoother surface with a roughness of just 4.9 nm, as compared with the TiO_x film and the CsO_x film. And, the double film provides a better adhesion with P3HT:ICBA blend solutions, evidenced by measurements of solution contact angles, which was found at the interface between P3HT:ICBA blend droplets and the CBLs. Afterwards, it is found that the highest electron mobility (μ_e) of 5.52×10^{-3} cm^2 $V^{-1} \cdot s^{-1}$ is achieved in inverted electron-only devices with TiO_x/CsO_x film measured with space-charge-limited current (SCLC) method. Moreover, current density-voltage (*J-V*) measurements show that the P3HT:ICBA inverted PSCs and the P3HT:PCBM inverted PSCs with TiO_x/CsO_x film exhibit a PCE of 5.65% and 3.76%, respectively, under the illumination of AM 1.5, 100

mW cm^{-2}, which is higher than that of the PSCs with TiO_x film and the PSCs with CsO_x film. The results indicate that the TiO_x/CsO_x is superior than the TiO_x and the CsO_x, not only for the better interfacial contact, but also for the achievement of the higher electron mobility, and thereby leading to an enhanced device performance. Finally, the TiO_x/CsO_x film possesses many advantages, such as 1) solution processability with ethanol and isopropanol solvents, which promote the application of solution-processing technologies, e.g., spin coating and role-to-role printing and 2) low cost since both TiO_x and CsO_x are cheap to produce and commonly used materials in organic photovoltaic and light-emitting fields, which suggests their huge potential for practical applications.

Methods

P3HT (4002-E) and PCBM were purchased from Rieke Metals Inc. (Lincoln, NE, USA) and Nano-C (Westwood, MA, USA), respectively. Indene-C_{60} bisadduct was purchased from Solarmer Inc. (El Monte, CA, USA). The TiO_x film was prepared by spin coating TiO_x sol-gel solution [22] on fluorinated tin oxide (FTO) substrate and then was thermally treated at 200°C for 30 min in air. Whereas, the CsO_x film was prepared by spin coating isopropanol solution of Cs_2CO_3 on FTO substrate and then thermal annealing at 160°C for 10 min in a glove box filled with Ar atmosphere. When spin coating the Cs_2CO_3 solution on FTO/TiO_x substrate and then thermal annealing at 160°C for 10 min, it forms the TiO_x/CsO_x film.

All the inverted PSCs were fabricated on FTO-coated glass. First, the different film was spin coated and then baked on FTO. Then, the blend solution of P3HT:PCBM and P3HT:ICBA in dichlorobenzene (1:1, *w*/*w*, 36 mg ml^{-1}) was spin coated at 800 rpm. The active layers were then placed into glass petri dishes to undergo solvent annealing and annealed at 150°C for 10 min on a hot plate in a glove box. Subsequently, MoO_3 (10 nm) and Al (100 nm) were evaporated as an anode buffer layer and anode, respectively, under the pressure of ≤1.0×10^{-4} Pa. Transmittance spectra were taken on a Hitachi U-3010 UV-visible spectrophotometer (Hitachi, Ltd., Chiyoda-ku, Japan). The surface morphology of active layers was characterized by AFM (SPM-9500J3, Shimadzu, Kyoto, Japan). The *J-V* measurement of the inverted PSCs was conducted on a computer-controlled Keithley 236 Source Measure Unit (Keithley Instruments, Inc., Cleveland, OH, USA). Device characterization was carried out in a glove box under illumination of AM 1.5 G, 100 mW cm^{-2} using a xenon-lamp-based solar simulator (from Newport Co., LTD., Irvine, CA, USA).

Results and discussion

To investigate the effect of the cathode buffer layers on the performance of the inverted PSCs, we designed six types of inverted PSC devices with different structures:

(A). FTO/CsO_x/P3HT:ICBA (200 nm)/MoO_3 (10 nm)/Al (100 nm),
(B). FTO/TiO_x(80 nm)/P3HT:ICBA (200 nm)/MoO_3 (10 nm)/Al (100 nm),
(C). FTO/TiO_x(80 nm)/CsO_x/P3HT:ICBA (200 nm)/MoO_3 (10 nm)/Al (100 nm),
(D). FTO/CsO_x/P3HT:PCBM (200 nm)/MoO_3 (10 nm)/Al (100 nm),
(E). FTO/TiO_x (80 nm)/P3HT:PCBM (200 nm)/MoO_3 (10 nm)/Al (100 nm),
(F). FTO/TiO_x(80 nm)/CsO_x/P3HT:PCBM (200 nm)/MoO_3 (10 nm)/Al (100 nm).

Device performance

Figure 2a shows the *J-V* characteristic curves of the P3HT:ICBA inverted PSCs with a film of TiO_x, CsO_x, and TiO_x/CsO_x under simulated AM 1.5 G solar illumination of 100 mW cm^{-2}. For comparison, more than 30 solar cells were fabricated and characterized to confirm the performance trends. It presents that the inverted PSCs with CsO_x film (devices A) show a relatively poor PCE of 4.91%

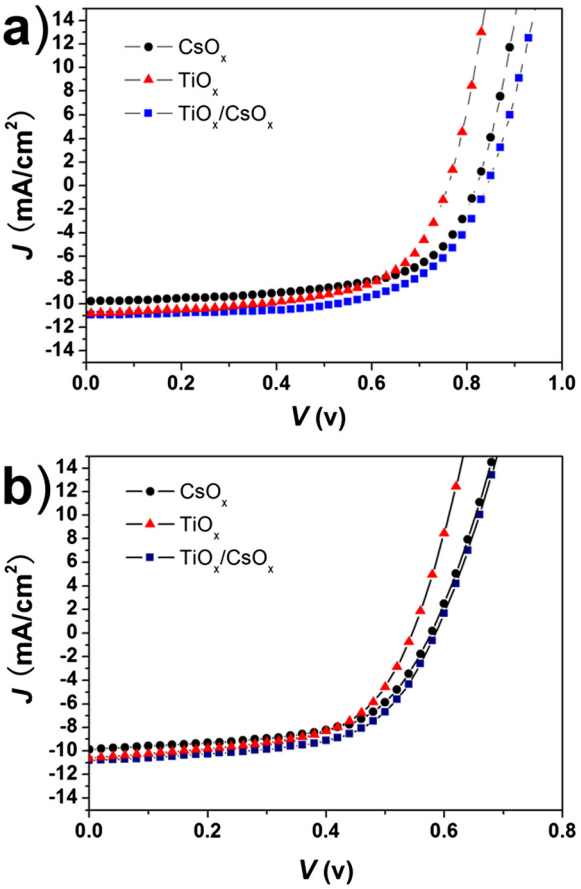

Figure 2 *J-V* **characteristics of the P3HT:ICBA-based inverted PSCs (a) and the P3HT:PCBM-based inverted PSCs (b) with different film, respectively.**

with V_{OC} of 0.82 V, J_{SC} of 9.79 mA cm^{-2}, and fill factor (*FF*) of 61.2%. Compared with the devices A, the PSCs with TiO_x film (devices B) yield an equipotent PCE of 4.95%, with a lower V_{OC} of 0.76 V, a higher J_{SC} of 10.82 mA cm^{-2}, and a *FF* of 60.2%. It is considered that the higher J_{SC} of 10.82 mA cm^{-2} is attributed to the exciton- and hole-blocking ability of the TiO_x film resulted from its favorable conduction band, as shown in Figure 1b. For the PSCs with the TiO_x/CsO_x film (devices C), the highest PCE of 5.65% is achieved with V_{OC} of 0.84 V, J_{SC} of 10.95 mA cm^{-2}, and *FF* of 61.4%, demonstrating a good combination of TiO_x and CsO_x, which compensates the loss in V_{OC} of devices B as well as in J_{SC} of devices A, respectively. Such photovoltaic performance parameters of the inverted PSCs are summarized in Table 1.

To further investigate the general suitability of the TiO_x/CsO_x film in inverted PSCs, the other electron acceptor material of PCBM was used instead of ICBA for fabricating P3HT:PCBM inverted PSCs. The *J-V* characteristic curve is shown in Figure 2b. As expected, for the inverted PSCs with CsO_x film (devices D), a PCE of 3.41% is achieved with V_{OC} of 0.58 V, J_{SC} of 9.86 mA cm^{-2}, and *FF* of 59.6%. Compared with that of the devices D, the PCE and *FF* of the inverted PSCs with TiO_x film (devices E) just change a little, whereas the J_{SC} is enhanced significantly from 9.86 to 10.63 mA cm^{-2} and the V_{OC} drops severely from 0.58 to 0.55 V. The inverted PSCs with TiO_x/CsO_x film (devices F) exhibit a PCE of 3.76%, better than that of the devices D and the devices E, which may be due to more electron extraction from the P3HT:PCBM active layer to the FTO cathode. Note that compared with the devices D, the devices E yield an enhanced short-circuit current, maybe due to a better hole-transporting and electron-blocking property of the TiO_x than that of the CsO_x. When TiO_x/CsO_x was used as a cathode buffer layer, it did not induce an increase in J_{SC}; however, a significant increase in V_{OC} from 0.76 to 0.84 V was observed clearly, attributed to the insert of CsO_x film with a low work function. The changes in J_{SC} and V_{OC} of the P3HT:PCBM inverted PSCs agree with those of the P3HT:ICBA inverted PSCs.

Optical properties and surface morphology of the films

Figure 3 shows the optical transmittance of CsO_x, TiO_x, and TiO_x/CsO_x on FTO substrates. The CsO_x film is highly transparent in the visible range, and the minimum light transmittance is not less than 90% between 400 and 800 nm. Compared with the CsO_x film on FTO substrate, the TiO_x film exhibits a decreased optical transmittance in the range of 300 to 800 nm, whereas the TiO_x/CsO_x has a decrease optical transmittance of 350 to 450 nm, as compared with the TiO_x, suggesting an ultra-thin film of CsO_x on the TiO_x surface.

To investigate the surface morphology of FTO modified by the film, atomic force microscopy measurements were carried out. Figure 4 shows the surface images of the four samples, including the FTO substrate, TiO_x, CsO_x, and TiO_x/CsO_x film on FTO substrate. It presents that the FTO substrate without any modification by CsO_x or TiO_x shows a lot of large 'valleys' and the root mean square (RMS) is about 15.7 nm. After spin coating Cs_2O_3 solution on the FTO substrate and then thermal annealing, it forms a CsO_x thin film, which exhibits a lower RMS of 12.5 nm; however, there is not any apparent change in surface morphology between the FTO and the CsO_x-modified FTO. Due to the modification of TiO_x on FTO substrate, the TiO_x film exhibits a decreased RMS of about 7.6 nm. Moreover, it shows smaller 'valleys' on the surface and becomes much smoother than the CsO_x film, whereas the TiO_x/CsO_x film presents a RMS of just 4.9 nm, indicating the CsO_x combines well with the TiO_x film.

Note that it is difficult to directly measure the thickness of the CsO_x film on the top of TiO_x film because the thickness of the CsO_x film is much smaller than the RMS of either the FTO substrate or the TiO_x film. However, the varieties of surface morphology in the four samples have been probed by AFM measurements, implying the presence of the CsO_x layer on FTO substrates as well as TiO_x-modified FTO substrates.

Droplet contact angle measurements

Due to the device performance being significantly dependent on the interfacial contact property of the

Table 1 Summary of performance of the P3HT:ICBA inverted PSCs and the P3HT:PCBM inverted PSCs with different film

Device	V_{OC} (V)	J_{SC} (mA cm^{-2})	*FF* (%)	PCE (%)	Contact angle (°)	μ_e (cm^2 V^{-1}·s^{-1})
CsO_x[a]	0.82	9.79	61.2	4.91	24.5 ± 0.5	3.85×10^{-3}
TiO_x[a]	0.76	10.82	60.2	4.95	32.0 ± 2.0	5.00×10^{-3}
TiO_x/CsO_x[a]	0.84	10.95	61.4	5.65	21.0 ± 0.5	5.52×10^{-3}
CsO_x[b]	0.58	9.86	59.6	3.41	—	—
TiO_x[b]	0.55	10.63	57.3	3.35	—	—
TiO_x/CsO_x[b]	0.59	10.81	59.0	3.76	—	—

[a]PSCs based on P3HT:ICBA; [b]PSCs based on P3HT:PCBM.

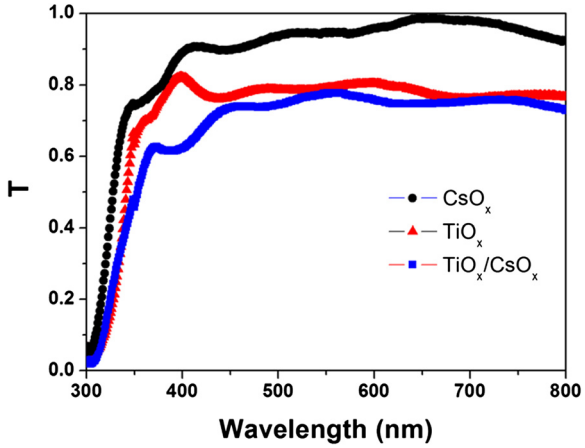

Figure 3 Optical transmittance of the films of TiO_x, CsO_x, and TiO_x/CsO_x, respectively.

film/active layer [40], which contributes to surface energy, it is necessary to observe the surface energy of the film. In this work, the surface energy of the film is studied with measurements of solution contact angles between a drop of P3HT:ICBA solution and the different film. For observing distinctly the interfacial contact angles, we used directly the P3HT and ICBA blend solution (1:1, *w*/*w*, 36 mg ml^{-1}) in dichlorobenzene as the 'solution' and measured the contact angles between the solution drop and the different film. Figure 5 shows the droplet images of P3HT:ICBA solutions on FTO substrate, CsO_x, TiO_x, and TiO_x/CsO_x film, respectively. It presents that the contact angle of the FTO surface to the P3HT:ICBA blend solution is 46.5° ± 2.5°, indicating a poor binding of the blend droplet to the FTO surface. Moreover, compared with the droplet on the FTO substrate, the smaller contact angle of 32.0° ± 2.0° and 24.5° ± 0.5° is observed for the droplet on the TiO_x and the CsO_x film, respectively, indicating a better wetting of the solvent, whereas the blend droplet has the smallest contact angle of just 21.0° ± 0.5° to the TiO_x/CsO_x film, suggesting the best affinity of the P3HT:ICBA active layer to the TiO_x/CsO_x film, which will be electrically/energetically favorable to the electron extraction and hence facilitates the fabrication of efficient inverted PSCs [29].

The RMS value of the TiO_x, CsO_x, and TiO_x/CsO_x is 12.5, 7.6, and 4.9 nm, respectively, and the corresponding P3HT:ICBA solution contact angle is 32.0° ± 2.0°, 24.5° ± 0.5°, and 21.0° ± 0.5°, respectively, suggesting that the contact angle decreases with the decrease of the RMS value. The change of the solution contact angle is partially resulted from the morphology variation induced by the CsO_x modification. In the work, the factor of RMS alters the interfacial contact angles and induces an enhancement of wetting and adhesion by changing surface energy, as also reported in previous literature [40].

Electron mobility measurements

The electron-extraction ability by the different film may be significantly dependent on the interface contact property and the energy-level alignment. To precisely assess the correlation among the factors, we have carefully examined the μ_e of electron-only devices with different

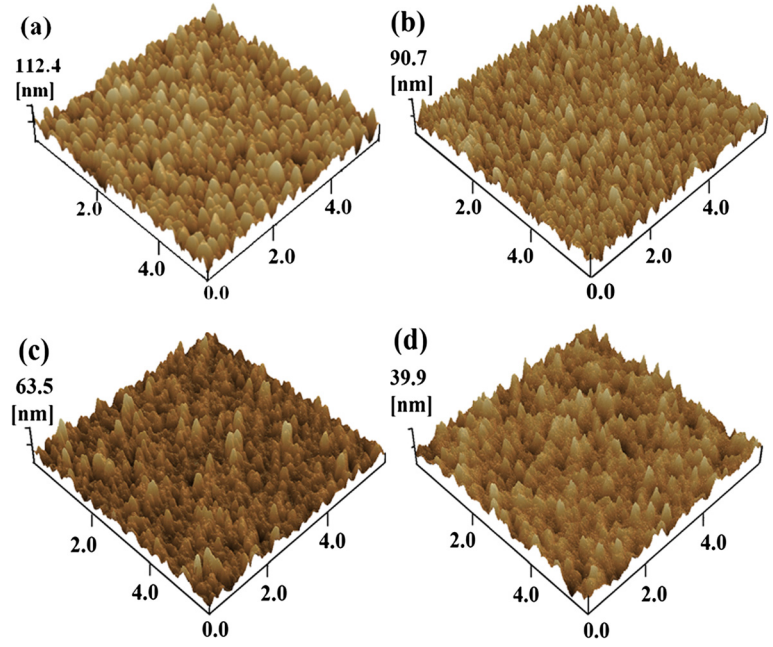

Figure 4 Surface morphology of FTO substrate (a), TiO_x (b), CsO_x (c), and TiO_x/CsO_x (d), respectively. The scan size is 6 μm × 6 μm.

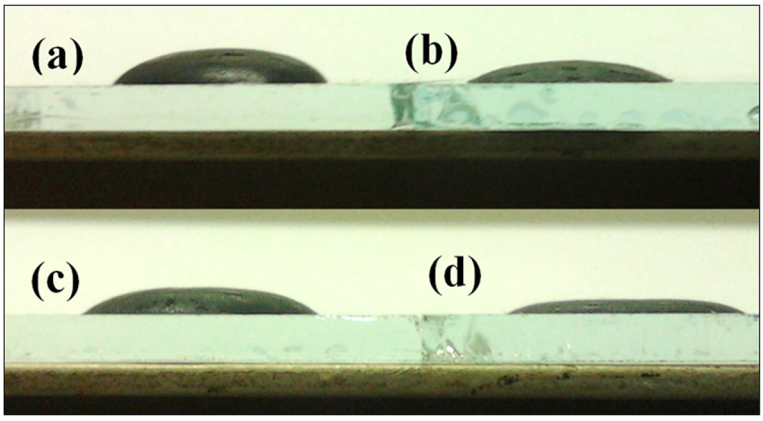

Figure 5 Droplet images of P3HT:ICBA solution. Droplet images of P3HT:ICBA solution on the surface of FTO substrate **(a)**, CsO_x **(b)**, TiO_x **(c)**, and TiO_x/CsO_x **(d)**, respectively. The length of the FTO-coated glass substrate is 3.0 cm.

film by using the SCLC method. In the work, the electron-only devices with an architecture of ITO/CBL/P3HT:ICBA/CsO_x/Al were fabricated to measure the μ_e. In such electron-only devices, the TiO_x, CsO_x, and TiO_x/CsO_x is used as a CBL, whereas the CsO_x layer on the active layer surface is employed as a hole-blocking layer. Note that it is spin coated with Cs_2CO_3 solution and then thermally annealed for 160°C for 10 min in glove box filled with Ar. Generally, high performance of PSCs commonly accompanies with a high-electron mobility, which is mainly influenced by exciton dissociation, as well as charge-carrier recombination at the interfaces of donor/acceptor and the interfaces of CBL/acceptor. The single-carrier mobility can be obtained from the J_{SCLC}-V^2 curve (Figure 6) by the SCLC method using the Mott-Gurney square law [41]:

$$J_{SCLC} = \frac{9}{8}\varepsilon_r \varepsilon_0 \mu \frac{V^2}{L^3} \quad (1)$$

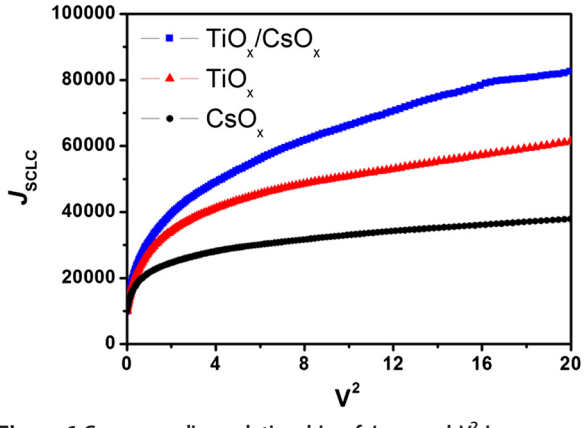

Figure 6 Corresponding relationship of J_{SCLC} and V^2 in electron-only devices with different film.

where ε_r is the dielectric constant of the material; ε_0 is the permittivity of free space; L is the distance between the cathode and anode, which is equivalent to the film thickness; and V is the applied voltage. Figure 6 shows the SCLC curves of the P3HT:ICBA-based electron-only devices with different film. It demonstrates the corresponding relationship of J_{SCLC} with V^2, where J_{SCLC} is the dark current density. The μ_e of the devices with CsO_x film is only 3.85×10^{-3} cm^2 $V^{-1} \cdot s^{-1}$. Compared with the device with a CsO_x film, however, the devices with TiO_x/CsO_x film show an enhanced remarkable μ_e of 5.52×10^{-3} cm^2 $V^{-1} \cdot s^{-1}$, suggesting an enhanced electron-extraction ability by the TiO_x/CsO_x film and hence leading to the enhancement in J_{SC} and PCE of the inverted PSCs. It should be noted that the μ_e values of the inverted PSCs were higher than those of normal PSCs in previous work [42]. The data are summarized in Table 1. In the work, the increase of the μ_e should be also related to the reduction in work function of the TiO_x surface modified by CsO_x. Li et al. reckoned that a thin layer of CsO_x is capable of lowering the work function of the underlying layer of ITO [27]. Moreover, Xu et al. reported inverted PSCs with a component film of Cs_2CO_3:4,7-Diphenyl-1,10-phenanthroline (BPhen) [43]. The work function of pristine BPhen on the ITO substrate was determined to be 3.1 eV by ultraviolet photoelectron spectroscopy, while the corresponding work function of the Cs_2CO_3:BPhen component layer was reduced to about 2.6 eV, thereby leading an increase in V_{OC} from 0.40 to 0.64 V and J_{SC} from 7.3 to 9.4 mA cm^{-2} of inverted PSCs with Cs_2CO_3:BPhen film as compared to inverted PSCs with BPhen film [43]. Combining all the above and our mentioned results, it is believed that the CsO_x (or Cs_2CO_3)-modified film can reduce the WF of the film and provide a better wetting property of the blend solvent on the TiO_x/CsO_x film surface, as well as a favorable energy-level alignment, which facilitate electron

injection from electron acceptor to cathode, and thus leading to a remarkable improvement in V_{OC} and J_{SC}.

Conclusions

In summary, high-efficiency inverted polymer solar cells are demonstrated with a solution-processed TiO_x/CsO_x layer as a cathode buffer layer. By inserting a CsO_x film at the interface of the TiO_x/active layer, the power conversion efficiency up to 5.65% and 3.76% has been achieved in inverted PSCs with P3HT:ICBA and inverted PSCs with P3HT:PCBM, respectively, under 100-mW cm^{-2} AM 1.5 G simulated solar illumination, suggesting that the TiO_x/CsO_x is superior than the TiO_x and the CsO_x. Moreover, this work not only provides a new option for the selection of the solution-processed cathode buffer layer in designing efficient and stable inverted PSCs, but also presents that the improvement of the interface contact property is also an essential factor for efficient polymer solar cells when preparing cathode buffer layers.

Competing interests

The authors declare that they have no competing interests.

Authors' contributions

XZ and XF designed the experiments and carried out the synthesis and characterization of the samples. XZ analyzed the results and wrote the first draft of the manuscript. XF and XS participated in analyses of the results and discussion of this study. YZ and ZZ revised the manuscript and corrected the English. All authors read and approved the final manuscript.

Acknowledgements

This work was supported by the National Nature Science Foundation of China (No. 11405280), the Foundation from Education Department of Henan Province of China (No. 14B140021), and the Startup Foundation for Doctors of Zhoukou Normal University of China (zksybscx201210).

Author details

[1]School of Physics and Electromechnical Engineering, Zhoukou Normal University, Zhoukou 466001, People's Republic of China. [2]Hubei Collaborative Innovation Center for Advanced Organic Chemical Materials, Faculty of Physics and Electronic Science, Hubei University, Wuhan 430062, People's Republic of China.

Received: 26 November 2014 Accepted: 13 January 2015
Published online: 31 January 2015

References

1. Peet J, Heeger AJ, Bazan GC. "Plastic" solar cells: self-assembly of bulk heterojunction nanomaterials by spontaneous phase separation. Acc Chem Res. 2009;42:1700–8.
2. Li G, Tao Y, Yang H, Shrotriya V, Yang G, Yang Y. "Solvent annealing" effect in polymer solar cells based on poly(3-hexylthiophene) and methanofullerenes. Adv Funct Mater. 2007;17:1636–44.
3. Mauger SA, Chang LL, Friedrich S, Rochester CW, Huang DM, Wang P, et al. Self-assembly of selective interfaces in organic photovoltaics. Adv Funct Mater. 2013;23:1935–46.
4. Krebs FC. Fabrication and processing of polymer solar cells: a review of printing and coating techniques. Solar Energy Materials Solar Cells. 2009;93:394–412.
5. Chen JW, Cao Y. Development of novel conjugated donor polymers for high-efficiency bulk-heterojunction photovoltaic devices. Acc Chem Res. 2009;42:1709–18.
6. Chen YJ, Yang SH, Hsu CS. Synthesis of conjugated polymers for organic solar cell applications. Chem Rev. 2009;109:5868–923.
7. Li YF. Molecular design of photovoltaic materials for polymer solar cells: towards suitable electronic energy levels and broad absorption. Acc Chem Res. 2012;45:723–33.
8. Fan X, Wang JZ, Huang HH, Wang H. Binary additives regulate the $PC_{71}BM$ aggregate morphology for highly efficient polymer solar cells. ACS Photonics. 2014;1:1278–84.
9. Chen HY, Hou JH, Zhang SQ, Liang YY, Yang GW, Yang Y, et al. Polymer solar cells with enhanced open-circuit voltage and efficiency. Nat Photonics. 2009;3:649–53.
10. Liang YY, Xu Z, Xia JB, Tsai ST, Wu Y, Li G, et al. For the bright future-bulk heterojunction polymer solar cells with power conversion efficiency of 7.4%. Adv Mater. 2010;22:E135–8.
11. Huo LJ, Zhang SQ, Guo X, Xu F, Li YF, Hou JH. Replacing alkoxy groups with alkylthienyl groups: a feasible approach to improve the properties of photovoltaic polymers. Angew Chem Int Ed. 2011;50:9697–702.
12. Price S, Stuart A, Yang L, Zhou H, You W. Fluorine substituted conjugated polymer of medium band gap yields 7% efficiency in polymer-fullerene solar cells. J Am Chem Soc. 2011;133:4625–31.
13. Chu T, Lu J, Beaupre S, Zhang Y, Pouliot J, Wakim S, et al. Bulk heterojunction solar cells using thieno [3, 4-c] pyrrole-4, 6-dione and dithieno [3, 2-b: 2′, 3′-d] silole copolymer with a power conversion efficiency of 7.3%. J Am Chem Soc. 2011;133:4250–3.
14. Small CE, Chen S, Subbiah J, Amb CM, Tsang SW, Lai TH, et al. High-efficiency inverted dithienogermole-thienopyrrolodione-based polymer solar cells. Nat Photonics. 2012;6:115–20.
15. Dou L, You J, Yang J, Chen CC, He Y, Murase S, et al. Tandem polymer solar cells featuring a spectrally matched low-band gap polymer. Nat Photonics. 2012;6:180–5.
16. Irwin MD, Buchholz DB, Hains AW, Chang RPH, Marks TJ. p-type semiconducting nickel oxide as an efficiency-enhancing anode interfacial layer in polymer bulk-heterojunction solar cells. Proc Natl Acad Sci U S A. 2008;105:2783–7.
17. Jørgensen M, Norrman K, Krebs FC. Stability/degradation of polymer solar cells. Solar Energy Materials Solar Cells. 2008;92:686–714.
18. Hau SK, Cheng YJ, Yip HL, Zhang Y, Ma H, Jen AKY. Effect of chemical modification of fullerene-based self-assembled monolayers on the performance of inverted polymer solar cells. ACS Appl Mater Interfaces. 2010;2:1892–902.
19. Gadisa A, Liu Y, Samulski ET, Lopez R. Role of thin n-type metal-oxide interlayers in inverted organic solar cells. ACS Appl Mater Interfaces. 2012;4:3846–51.
20. Shao SY, Zheng K, Pullerits T, Zhang FL. Enhanced performance of inverted polymer solar cells by using poly(ethylene oxide)-modified ZnO as an electron transport layer. ACS Appl Mater Interfaces. 2013;5:380–5.
21. Kuwabara T, Iwata C, Yamaguchi T, Takahashi K. Mechanistic insights into UV-induced electron transfer from PCBM to titanium oxide in inverted-type organic thin film solar cells using AC impedance spectroscopy. ACS Appl Mater Interfaces. 2010;2:2254–60.
22. Salim T, Yin ZY, Sun S, Huang X, Zhang H, Lam YM. Solution-processed nanocrystalline TiO_2 buffer layer used for improving the performance of organic photovoltaics. ACS Appl Mater Interfaces. 2011;3:1063–7.
23. Lin ZH, Jiang CY, Zhu CX, Zhang J. Development of inverted organic solar cells with TiO_2 interface layer by using low-temperature atomic layer deposition. ACS Appl Mater Interfaces. 2013;5:713–8.
24. Fan X, Fang GJ, Guo SS, Liu NS, Gao HM, Qin PL, et al. Controllable synthesis of flake-like Al-doped ZnO nanostructures and its application in inverted organic solar cells. Nanoscale Res Lett. 2011;6:546.
25. Zhang FL, Ceder M, Inganäs O. Enhancing the photovoltage of polymer solar cells by using a modified cathode. Adv Mater. 2007;19:1835–8.
26. Jiang CY, Sun XW, Zhao DW, Kyaw AKK, Li YN. Low work function metal modified ITO as cathode for inverted polymer solar cells. Solar Energy Materials Solar Cells. 2010;94:1618–21.
27. Li G, Chu CW, Shrotriya V, Huang J, Yang Y. Efficient inverted polymer solar cells. Appl Phys Lett. 2006;88:253503.
28. Cui CH, Fan X, Zhang MJ, Zhang J, Min J, Li YF. A D–A copolymer of dithienosilole and a new acceptor unit of naphtho[2,3-c]thiophene-4,9-dione for efficient polymer solar cells. Chem Commun. 2011;47:11345–7.
29. Cheng G, Tong WY, Low KH, Che CM. Thermal-annealing-free inverted polymer solar cells using ZnO/Cs_2CO_3 bilayer as electron-selective layer. Solar Energy Materials Solar Cells. 2012;103:164–70.

30. Fan X, Cui CH, Fang GJ, Wang JZ, Li SZ, Cheng F, et al. Efficient polymer solar cells based on poly(3-hexylthiophene):indene-C_{70} bisadduct with a MoO_3 buffer layer. Adv Funct Mater. 2012;22:585–90.
31. Fan X, Fang GJ, Cheng F, Qin PL, Huang HH, Li YF. Enhanced performance and stability in PBDTTT-C-T:$PC_{70}BM$ polymer solar cells by optimizing thickness of NiO_x buffer layers. J Phys D Appl Phys. 2013;46:305106.
32. Cheng F, Fang GJ, Fan X, Huang HH, Zheng Q, Qin PL, et al. Enhancing the performance of P3HT:ICBA based polymer solar cells using LiF as electron collecting buffer layer and UV–ozone treated MoO_3 as hole collecting buffer layer. Solar Energy Materials Solar Cells. 2013;110:63–8.
33. Heo SW, Lee E, Seong KW, Moon DK. Enhanced stability in polymer solar cells by controlling the electrode work function via modification of indium tin oxide. Solar Energy Materials Solar Cells. 2013;115:123–8.
34. Li SS, Chen CW. Polymer–metal-oxide hybrid solar cells. e. 2013;1:10574–91.
35. He YJ, Chen HY, Hou JH, Li YF. Indene-C_{60} bisadduct: a new acceptor for high performance polymer solar cells. J Am Chem Soc. 2010;132:1377–82.
36. He YJ, Zhao GJ, Peng B, Li YF. High yield synthesis, electrochemical and photovoltaic properties of indene-C_{70} bisadduct. Adv Funct Mater. 2010;20:3383–9.
37. Schmidt H, Zilberberg K, Schmale S, Flügge H, Riedl T, Kowalsky W. Transient characteristics of inverted polymer solar cells using titaniumoxide interlayers. Appl Phys Lett. 2010;96:243305.
38. Kuwabara T, Nakayama T, Uozumi K, Yamaguchi T, Takahashi K. Highly durable inverted-type organic solar cell using amorphous titanium oxide as electron collection electrode inserted between ITO and organic layer. Solar Energy Materials Solar Cells. 2008;92:1476–82.
39. Yang Q, Yang D, Zhao S, Huang Y, Xu Z, Liu X, et al. The improved performance of solution-processed SQ:$PC_{71}BM$ photovoltaic devices via MoO_3 as the anode modification layer. Appl Surf Sci. 2013;284:849–54.
40. Kyaw AKK, Sun XW, Jiang CY, Lo GQ, Zhao DW, Kwong DL. An inverted organic solar cell employing a sol–gel derived ZnO electron selective layer and thermal evaporated MoO_3 hole selective layer. Appl Phys Lett. 2008;93:221107.
41. Jung JW, Jo WH. Annealing-free high efficiency and large area polymer solar cells fabricated by a roller painting process. Adv Funct Mater. 2010;20:2355–63.
42. Fan X, Li SZ, Guo SS, Fang GJ. Understanding the phase separation evolution in efficient P3HT : IC70BA-based bulk-heterojunction polymer solar cells. J Phys D Appl Phys. 2013;46:055502.
43. Xu ZQ, Yang JP, Sun FZ, Lee ST, Li YQ, Tang JX. Efficient inverted polymer solar cells incorporating doped organic electron transporting layer. Org Electron. 2012;13:697–704.